The curious case of a strong relationship between ENSO and Indian summer monsoon in CFSv2 model

Priyanshi Singhai[1,2], Arindam Chakraborty[1,2,3], Kaushik Jana[4], Kavirajan Rajendran[5]and Sajani Surendran[5]

[1]Centre for Atmospheric and Oceanic Sciences, Indian Institute of Science, Bengaluru, 560012, India

[2]Divecha Centre for Climate Change, Indian Institute of Science, Bengaluru, 560012, India

[3]DST-Centre of Excellence in Climate Change, Divecha Centre for Climate Change, Indian Institute of Science, Bengaluru 560012, India.

[4]Mathematical and Physical Sciences Division, Ahmedabad University, Ahmedabad-380009, India

[5]CSIR Fourth Paradigm Institute (CSIR-4PI), Bangalore-560037, India

Key Points:

- In CFSv2, the consensus on ENSO forcing sign among ensemble members effectively represents ENSO's influence in the ensemble mean.

- Non-ENSO climate forcings, despite being present in individual members, vary considerably, attenuating non-ENSO signals in the ensemble mean.

- Hence, the ensemble mean shows a strong ENSO-ISMR correlation, while individual ensemble members do not exhibit the same relationship.

Corresponding author: Priyanshi Singhai, `priyanshis@iisc.ac.in`, `pspriyanshi66@gmail.com`

Abstract

An ensemble of forecasts is necessary to identify the uncertainty in predicting a non-linear system like climate. While ensemble averages are often used to represent the mean state and diagnose physical mechanisms, they can lead to information loss and inaccurate assessment of the model's characteristics. We highlight an intriguing case in the seasonal hindcasts of the Climate Forecast System version-2. While all ensemble members often agree on the sign of predicted El Nino Southern Oscillation (ENSO) for a particular season, non-ENSO climate forcings, although present in individual members, are disparate. As a result, an ensemble mean retains ENSO anomalies while diminishing non-ENSO signals. This difference between ENSO and non-ENSO predictions and a more decisive impact of ENSO on seasonal climate increases the ensemble mean ENSO-Indian Summer Monsoon Rainfall correlation. Thus, a model's teleconnection skills, which often help interpret physical mechanisms, should be studied using individual members rather than ensemble averages.

Plain Language Summary

When it comes to predicting a chaotic system like climate, we generate a set of forecasts known as an ensemble. Each forecast in the ensemble starts from slightly different initial conditions. To evaluate the performance of the climate model, we often calculate the average of the ensemble. But only looking at the ensemble average can sometimes overlook important information and make our evaluations of the climate model less accurate. Here, we presented one such example where the ensemble mean fails to represent the true characteristic of the model. Previous studies reported that the year-to-year variations of the Indian summer monsoon rainfall in many climate models are heavily influenced by the climate of the central and eastern Pacific oceans. However, our analysis reveals that this relationship stems from the methodology used to compute ensemble mean rather than being an inherent characteristic of the model. Hence, our study highlights the importance of examining individual ensemble members to evaluate the models' forecasting abilities.

1 Introduction

Ensemble forecasting has become widely adopted for predicting inherently chaotic and non-linear systems like weather and climate (Molteni et al., 1996; Palmer, 2000). This approach involves running a numerical prediction model multiple times with different initial conditions or numerical atmospheric representations to address forecast uncertainty (Palmer, 2000; Leutbecher & Palmer, 2008; Weisheimer et al., 2011). Moreover, ensemble averages of forecasts are commonly used to address systematic model errors and represent forecasts as anomalies. This approach relies on the forecast value for a specific start time, lead time, and target period. However, there can be challenges if a forecast ensemble mean is needed for start times that are not included in the hindcasts or if the number of hindcasts is considerably smaller than the variance of the forecast anomaly (Tippett et al., 2018). Despite these challenges, numerous studies have extensively utilized this method to evaluate the model's teleconnection patterns and forecast skill in simulating Indian summer monsoon rainfall (ISMR).

The year-to-year variation of ISMR is primarily influenced by low-frequency variations in tropical sea surface temperatures (Charney & Shukla, 1981), particularly El Nino Southern Oscillation (ENSO) (Rasmusson & Carpenter, 1983; J. Shukla & Wallace, 1983). However, the impact of these SST variations on monsoons can vary due to the inherent chaotic nature of the climate system. Hence, the generation of ensemble forecasts becomes imperative to estimate the uncertainty associated with the ISMR predictions and to evaluate the model performance in predicting monsoons. Many of the climate models like ECMWF-SYSTEM4, North American Multi-Model Intercomparison Project (NMME), and CMIP models heavily rely on ENSO for ISMR prediction (Kim et al., 2012; Pillai et al., 2021; He et al., 2022; Rajendran et al., 2022). Interestingly, some models exhibit an ENSO-ISMR relationship that is nearly twice as strong as observed (Singh et al., 2019). For example, many coupled models of CMIP5 show a similar strong association, which attributes it to the westward shift of the anomalous low-level anticyclonic circulation over the tropical Indian

Ocean and western subtropical northwest Pacific. This shift causes an advection of dry air from the extratropics to the Indian region, causing a stronger ENSO-ISMR relationship (Ramu et al., 2018). The NCEP Climate Forecast system version-2 (CFSv2) model also demonstrates an overestimation of this relationship (George et al., 2016; Chattopadhyay et al., 2016), potentially due to an underestimation of synoptic activity over the Bay of Bengal in August, which amplifies the impact of ENSO on ISMR in the model (Das et al., 2022). Furthermore, the ENSO-ISMR relationship in the CFSv2 might also be influenced by SST biases in the equatorial central Pacific and Indian oceans (R. P. Shukla & Huang, 2016). Another study highlighted that the observed fluctuation in the ENSO-ISMR correlation over a longer period could also be ascribed to sampling variability (Cash et al., 2017; Gershunov et al., 2001). This finding is shown using a large ECMWF Ensemble Prediction System ensemble. Several studies also examine the impact of another variability on ISMR in the CFSv2. One of these studies suggests that the model has a problem capturing the air-sea interaction over the Indian Ocean and low-level winds over the Indian region (Krishnamurthy, 2018). Additionally, another study by (Sabeerali et al., 2019) indicates that CFSv2 has poor predictive skills in forecasting the teleconnection between the Atlantic zonal mode and ISM.

Although the above studies analyzed the model's teleconnection patterns using the ensemble average of the forecast, relying solely on this approach could lead to the loss of valuable information embedded within the individual ensemble forecasts. Hence, our objective is to investigate whether the ensemble mean of the forecasts reflects the true behavior of the model or displays distinct characteristics when compared to the individual ensemble members. We also want to ascertain whether the model errors discussed earlier are a consequence of inherent limitations in the model or are influenced by the methodology employed to analyze the teleconnection patterns.

2 Model Description, Experimental Design, and Observational Data sets

We utilize the National Centers for Environmental Prediction (NCEP) CFSv2 model, which is fully coupled and includes the NCEP GFS (Global forecast system) for the atmospheric component, Geophysical Fluid Dynamics Laboratory Modular Ocean Model version 4 for the ocean model, a two-layer sea ice model, and a four-layer Noah land surface model (Saha et al., 2014). GFS has a horizontal resolution of 0.91°and 64 vertical levels. The model simulation is performed at the computing platform of Council for Scientific and Industrial Research (CSIR) Fourth Paradigm Institute, Bengaluru, following the experimental setup used by Rajendran et al. (2021) and Singhai et al. (2023). The model is integrated for nine months using five different initial conditions for the period of 1979–2016. The initial conditions include 00UTC of 21 April (member 1), 26 April (member 2), 1 May (member 3), 6 May (member 4), and 11 May (member 5). This is referred to as "Model 1" or M1 in this study. Additionally, to verify the M1 results, the study also analyzes 124 nine months of reforecast (referred to as "Model 2" or M2) initialized from CFS-based initial conditions every fifth day from 1 January to 31 May, with four reforecasts per day (00, 06, 12, 18 UTC) from 1982 to 2010 (Saha et al., 2010).

The objective of this study is to investigate the difference in the model's characteristics in individual ensemble members and their mean. We treat each of the initial conditions reforecasts as a distinct entity to obtain the characteristic of individual members (E_{all}). Conversely, we calculate the ensemble mean using the following approach:

By assuming the linear superposition of different forcings, such as ENSO, IOD, and ATL, on ISMR, we can express ISMR (P) as follows:

$$P = C_0 + \sum_{j=1}^{n} C_j f_j \tag{1}$$

where f_j is the jth forcing and C_j are constants. The term C_0 can be neglected with the removal of the climatological values.

If there are m members of an ensemble prediction system, the above equation applies separately to each of the ensemble members. Thus, the ensemble mean (E_M) for ISMR can be computed in the following way.

$$\bar{P} = \sum_{j=1}^{n} C_j \bar{f}_j \tag{2}$$

Here, C_j remains unchanged as it represents the model's characteristics, while $\bar{f}_j$ represents the ensemble mean forcing and is computed by averaging the values across each ensemble member, as shown below.

$$\bar{f}_j = \frac{1}{m} \sum_{i=1}^{m} f_i$$

For model validation against observations, we use the June-September (JJAS) averaged Extended reconstructed sea surface temperature (ER-SST) version 5 data to derive the ENSO index (Huang et al., 2017). The India Meteorological Department (IMD) monthly mean gridded rainfall dataset with a spatial resolution of $1°\times1°$ is used to calculate ISMR (Rajeevan et al., 2006). JJAS average GPCP (Global Precipitation Climatology Project) data is also utilized to depict changes in precipitation over land and ocean (Huffman et al., 2009).

Index calculation

The area-averaged rainfall over the region ($7.5°–27.5°$N, $70°–90°$E) during the boreal summer monsoon season is used to define ISMR (Parthasarathy et al., 1994). For ISMR computation, only land grid points are considered. The ENSO index is the area-average SST anomaly over the Nino 3.4 region ($5°$S–$5°$N, $170°$W–$120°$W). SST anomaly greater (less) than $0.5°$C ($-0.5°$C) is classified as El Nino (La Nina). The ATL is defined as the averaged SST anomaly over a region ($20°$S–Eq, $30°$W–$20°$E) (Kucharski et al., 2008, 2007). The positive (negative) phases of ATL are identified when the JJAS averaged values exceed one (less than minus one) standard deviation.

Likelihood histogram

The likelihood histogram displays the distribution of ensemble members exhibiting coherent behavior, with a threshold of $0°C$ for both the ENSO and ATL indices. For a particular year, we determine the maximum number of ensemble members showing the same sign of anomaly (>0 or <0). For instance, years where all five ensemble members showed either a positive or negative ENSO index, are grouped in bin 5, while the 4 and 3 contained years with fewer coherent members.

3 Results

ENSO has a strong relationship with ISMR, with a correlation coefficient of -0.58, as shown in Fig 1a. However, the majority of the climate models, including CFSv2, overestimate the impact of ENSO on boreal summer monsoon rainfall, as reported in previous studies (Kim et al., 2012; R. P. Shukla & Huang, 2016; He et al., 2022; Rajendran et al., 2022). These studies often use the ensemble average method to examine the teleconnection patterns in the seasonal and sub-seasonal prediction systems. Although this method effectively reduces the random variations or "noise" inherent in ensemble forecasts, it also results in the loss of important information. For instance, Figure 1a depicts the relationship between ENSO and ISMR for the CFSv2 models 1 (M1) and 2 (M2). This association is shown using both individual (E_{all}, yellow bars) and the mean of ensemble members (E_M, red bars). It should be noted that there is a significant difference in the ENSO-ISMR relationship computed from these two methods for both M1 and M2. The correlation coefficient (CC) for the E_{all} ($CC_{M1} = -0.55$ and $CC_{M2} = -0.58$) is comparable to that seen in the observation (CC$=-0.58$). However, the relationship is greatly overestimated for E_M, resulting in a high correlation coefficient of -0.7 (M1) and -0.88 (M2). Furthermore, despite model M2 having a significantly larger number of ensemble members compared to model M1, there is a greater disparity in the correlation coefficient between E_M and E_{all} for M2 than for M1. This suggests that the strong relationship between ENSO and ISMR in the CFSv2

model, as reported by previous literature, is not a characteristic inherent to the model but stems from the ensemble average method. In addition, it is worth noting that our primary finding remains robust and consistent regardless of the number of ensemble members used in models M1 and M2. This highlights the reliability of our results, despite the potential impact of the number of ensemble members on the efficacy of the ensemble average method (Atger, 1999).
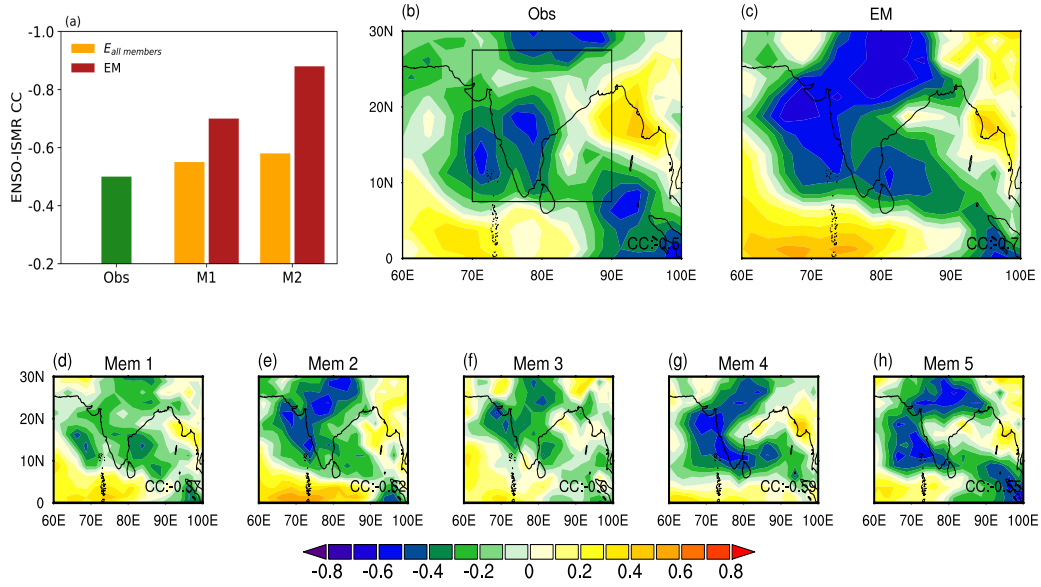

Figure 1. (a) The bar plot illustrates the relationship between ENSO and ISMR for the observation, as well as the CFSv2 models M1 (with 5 ensemble members) and M2 (with 124 ensemble members). This relationship is depicted using both individual members (E_{all}) and the ensemble mean (E_M) of the CFSv2 seasonal hindcasts. (b-h) The spatial composite of the correlation coefficient between the ENSO index and precipitation over the South Asian region. Panel (b) represents the observation, panel (c) shows the ensemble mean (E_M), and panels (d-h) present the correlation for all five individual ensemble members of model M1 (21 April (Mem 1), 26 April (Mem 2), 1 May (Mem 3), 6 May (Mem 4), and 11 May (Mem 5)). The inset value in (b-h) is for the correlation coefficient (CC) between ISMR and ENSO index for 1979-2016.

Figure 1b-h displays the spatial patterns showing the response of ENSO to ISMR for observation (Fig. 1b), ensemble mean (Fig. 1c), and the individual ensemble members (Fig. 1d-h) of model M1. Negative values of the correlation coefficient mark the entire Indian region in all three cases. However, these values are significantly higher for the ensemble mean

than for observation and other ensemble members. The negative values in the ensemble mean mainly concentrate on the western ghats and northern parts of the Indian region, particularly over the Indo-Gangetic belt (Fig 1c). The reason for such high negative values in the ensemble mean can be understood by examining the behavior of individual ensemble members. It is worth noting that the response of ENSO to ISMR varies significantly among ensemble members, ranging from -0.37 to -0.62. Member 1 displays the weakest ENSO response to ISMR with a CC of -0.37. In contrast, other members show a considerably strong relationship, albeit weaker than the ensemble mean. In addition, the negative CC among the ensembles, particularly for members 2, 4, and 5, are heterogeneously clustered over northern India. As a result, when the ensemble average is computed, the negative values are superimposed in a manner that causes the ENSO-ISMR relationship to be higher in the ensemble mean than in the individual members.
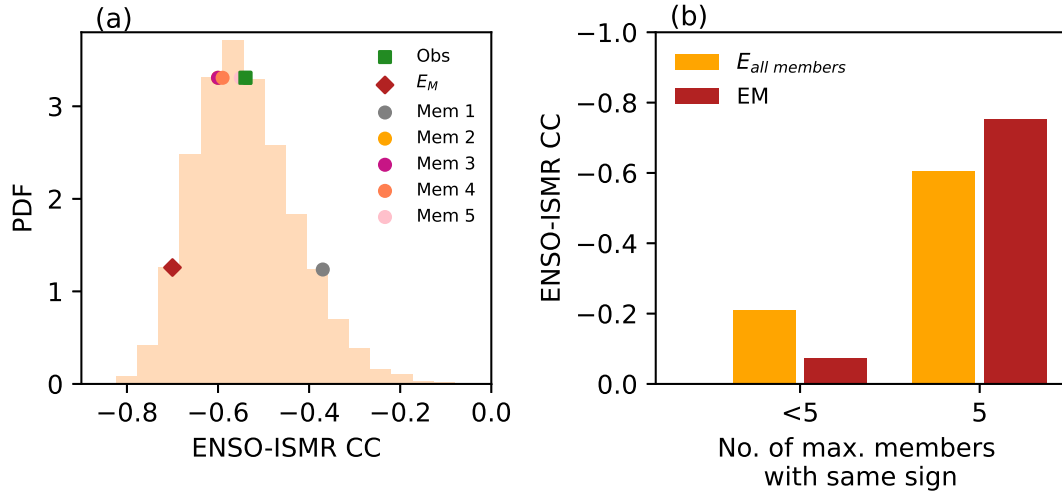

Figure 2. (a) The probability density function (PDF) of the correlation coefficient (CC) between ENSO forcing and Indian summer monsoon rainfall (ISMR). This analysis is based on a 38-year sample extracted from a total of 190 individual ensemble members. This process is randomized and repeated over 1000 iterations. Additionally, the CC values for the observation, the ensemble mean, and all five individual ensemble members (21 April (Mem 1), 26 April (Mem 2), 1 May (Mem 3), 6 May (Mem 4), and 11 May (Mem 5)) for the period of 1979–2016 are also indicated as markers. (b) The bar plot shows the ENSO-ISMR relationship when all 5 and less than 5 ensemble members exhibit the same sign of ENSO anomalies. The year distribution of the cases where there are 5 and <5 members having the same sign of ENSO anomalies are shown in Figure 3.

Figure 2a shows the probability distribution of the potential ENSO-ISMR correlation coefficients, generated by randomly selecting 38 years from the ensemble forecast of 190 years (38 years × five initial conditions). This process is randomized and repeated over 1000 times. Interestingly, the maximum likelihood of getting the correlation coefficient between ENSO-ISMR is −0.55 (mode), which is similar to the correlation corresponding to the observation and individual ensemble members. Additionally, four out of the five ensemble members are clustered around the mode value. The probability of getting the correlation coefficient of the ensemble mean (CC=−0.7) is much lower than that of CC computed using individual ensemble members (CC=−0.55). Once again, this finding confirms that the strong relationship between ENSO and ISMR observed in E_M is not an intrinsic feature of the CFSv2 model.
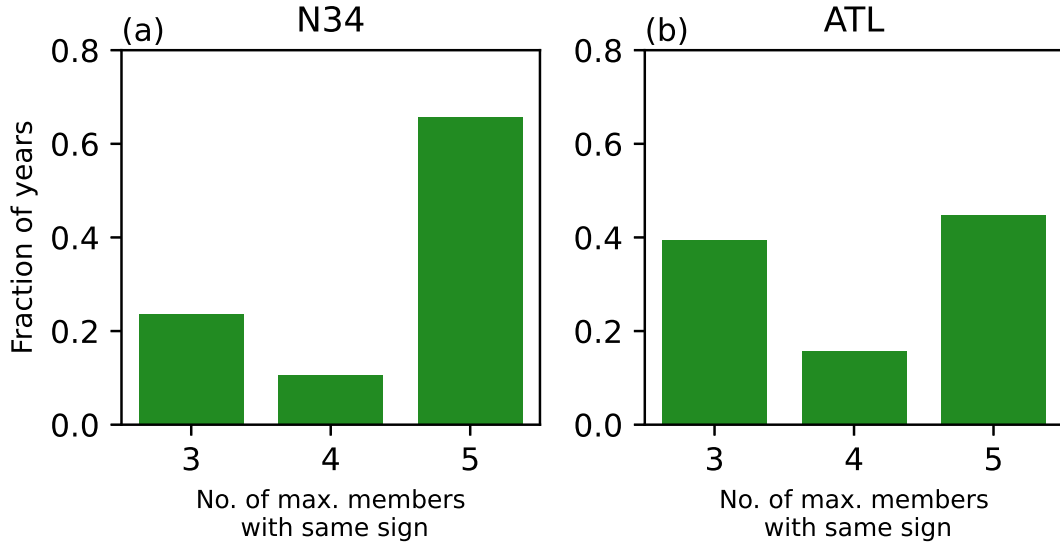

Figure 3. **The histograms show the distribution of the maximum number of ensemble members exhibiting the same signs of an anomaly for (a) ENSO Index (N34) and (b) Atlantic tropical variability (ATL).**

To investigate the differing response of ENSO on ISMR between the ensemble mean and individual ensemble members, we generate a histogram in Figure 3a to examine the behavior of each individual member under ENSO forcing. Additionally, since external forcings such as ATL can suppress the influence of ENSO on ISMR (Kucharski et al., 2008), the histogram

for ATL is also shown in Fig 3b. Our analysis shows that there is a high probability (around 66%) of obtaining the same sign of anomaly (either N34>0 or N34<0) by all five ensembles under ENSO forcing. Our analysis shows that there is a high probability (around 66%) of obtaining the same signs of anomaly (either N34>0 or N34<0) for each year across all five ensemble members under ENSO forcing. This leads to the ENSO forcing dominating the ensemble mean over individual members. As a result, the ENSO-ISMR relationship in the ensemble mean is majorly determined by these five coherent members (CC5=-0.77, Figure 2c). This leads to the retainment of the ENSO forcing in the ensemble mean, leading to a pronounced ENSO-ISMR relationship. This relationship in the ensemble mean is majorly determined by the years where all five ensemble members exhibit the coherent anomaly signs (CC5=-0.77, Figure 2c). In contrast, the contribution of members showing incoherent behavior (<5) is negligible ($CC_{<5} = -0.08$, Figure 2b). Notably, we also observe that the ENSO-ISMR relationship derived from the ensemble mean of the incoherent member (<5) is weaker than that computed from individual members (Fig 2b). This can be due to the cancellation of the ENSO forcing caused by the varying responses of ENSO among different ensemble members. On the other hand, for non-ENSO forcing, such as ATL, the likelihood of all five ensemble members exhibiting the same sign is much lower than ENSO forcing (Fig 3b). This may be due to non-linear processes over the Atlantic Oceans, contributing to the model's differing behavior among ensembles. Hence, in the case of non-ENSO forcing, even though it exists in individual members, it shows significant variability, resulting in the weakening of non-ENSO signals in the ensemble mean.

External climatic forcings such as ENSO and ATL tend to perturb the surface pressure patterns surrounding the Indian region, leading to modifications in the incoming and outgoing moisture fluxes (Chakraborty & Singhai, 2021). These fluxes, primarily from the Arabian Sea (F_W) and the Bay of Bengal (F_E), play a vital role in driving atmospheric convection over India during the boreal summer monsoon. Figure 4 shows a scatter plot that facilitates the examination of potential disparities in the responses of ENSO and ATL to moisture fluxes between individual members and the ensemble mean. To accomplish this,
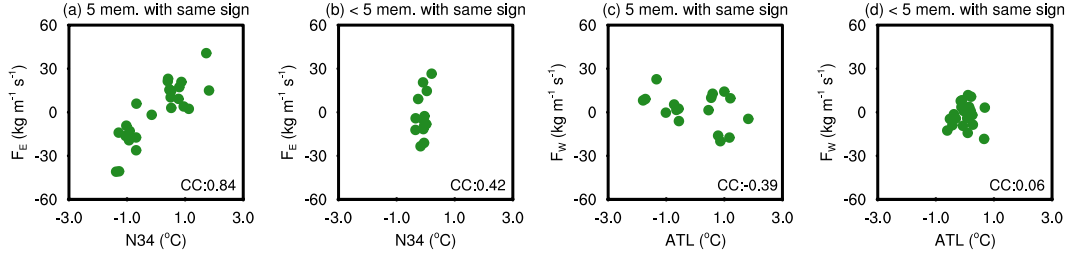
Figure 4. The scatter plots show the relationship between the ENSO index and moisture flux over the Bay of Bengal (F_E) when there is a maximum of (a) five and (b) less than five ensemble members with the same signs of ENSO anomaly. Similarly, in plots (c, d), we examine the relationship between ATL forcing and moisture flux over the Arabian Sea (F_W) for these two cases. To quantify the impact of ATL, we regress out the impact of ENSO from total moisture fluxes (explained in Supplementary Note 1).

we focus on dominant moisture fluxes such as F_E, which plays a crucial role in regulating

ENSO-driven rainfall in the model (Supplementary Figure 1), also shown by Singhai et al.

(2023) through analysis of individual ensemble members. Additionally, we examine the role

of F_W, the primary factor driving rainfall during ATL events (Supplementary Figure 2).

We then segregate the forcing and moisture fluxes based on years where five and less than

five members show the same sign of forcings (same way as in Figure 3). We notice that the

correlation between ENSO and F_E is higher in years when all members are coherent in sign

(CC=0.84) than in fewer coherent members (CC=0.42). Hence, the impact of F_E on the

ensemble mean is maintained when all members exhibit consistent signs, while its influence

diminishes when there are fewer members with coherent signs. Furthermore, as depicted in

Figure 4b, it is evident that the variability of ENSO forcing is significantly reduced when

fewer than five ensemble members exhibit the same sign, in contrast to the case when all

five members have coherent signs. It is due to the opposite signs of ENSO forcing in the in-

dividual ensemble members, which tend to cancel out each other, resulting in the decreased

variability of ENSO in the <5 case. As depicted in Figure 3b, the number of members

with coherent signs is lower for ATL than for ENSO. As a result, the impact of ATL in

the ensemble mean is reduced compared to ENSO. This reduction in ATL forcing leads to

a weaker response, as shown in Fig 4c and 4d. Moreover, similar to ENSO, the impact of

ATL forcing on F_W is more pronounced when all members have the same anomaly sign, as opposed to when there are fewer coherent sign members. This emphasizes that disparity in the impact of ENSO and ATL forcing on moisture fluxes between the ensemble mean and individual ensemble members is primarily influenced by the maximum number of ensemble members exhibiting a consistent sign of forcing.
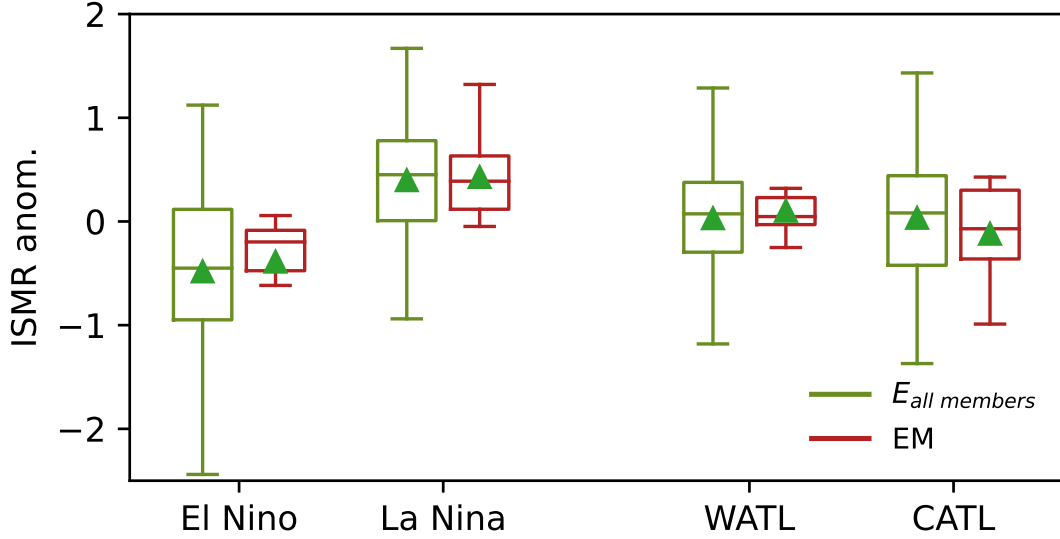

Figure 5. The box plot shows the ISMR response to positive and negative phases of ENSO (El Nino and La Nina) and ATL (Warm-ATL and Cold ATL) forcing.

Figure 5 illustrates the response of rainfall to positive and negative phases of ENSO and ATL in both the ensemble mean and individual ensemble members. The relationship between El Nino (La Nina) events and ISMR is observed to be different in the ensemble mean compared to the individual members, with almost all El Nino (La Nina) events leading to a decrease (increase) in ISMR in the former, but this is not the case in the latter. This difference is attributed to the high ENSO-ISMR relationship observed in the ensemble mean, which is a result of a maximum number of members exhibiting the coherent sign (as shown in Figure 3a). This finding also suggests that the model simulates the mean response of positive and negative ENSO phases to ISMR correctly. This response is largely governed by the climate of the Bay of Bengal (Singhai et al. (2023), Figure 4a). Conversely, similar to ENSO events, the rainfall variability sharply decreases in the ensemble mean compared

to the individual ensemble member during ATL events. This could be attributed to the suppressed effect of ATL forcing due to the negation of forcing caused by members having opposite anomaly signs. To summarize, the stronger relationship between ENSO and ISMR observed in the ensemble mean is primarily influenced by the agreement among ensemble members with the same ENSO anomaly sign. Nevertheless, the non-ENSO climate forcings present in individual members display substantial variability, leading to a reduction in the strength of non-ENSO signals within the ensemble mean.

4 Summary and discussions

The primary aim of this study is to address the critical issue of imprudent usage of the ensemble mean approach for evaluating the forecasting skills of climate models. It is observed that relying solely on the ensemble mean method neglects the valuable information embedded within individual ensemble members, potentially leading to erroneous evaluations of the model's teleconnection patterns. Our study highlights a notable case of a strong ENSO-ISMR relationship in the CFSv2 seasonal hindcasts. Previous studies have reported that the CFSv2 model, like many other climate forecast models, is subject to the strong influence of ENSO on ISMR (Kim et al., 2012; R. P. Shukla & Huang, 2016; He et al., 2022; Rajendran et al., 2022). Our analysis, however, suggests that this pronounced ENSO-ISMR relationship is primarily observed in the ensemble mean, while it is not apparent in the individual ensemble members. Hence, we aim to discern the underlying mechanisms contributing to the distinctive response of ENSO to ISMR in the ensemble mean versus individual ensemble members.

This observed discrepancy between the ensemble mean and individual ensemble members attributes to a change in the nature of forcing and its associated response during the computation of the ensemble mean. In particular, the strong relationship between ENSO and ISMR observe in the ensemble mean primarily stems from the consensus among ensemble members regarding the sign of ENSO anomaly. This retains the influence of ENSO

in the ensemble mean. Conversely, the significant variability of the non-ENSO forcings in individual members diminishes the strength of non-ENSO signals within the ensemble mean.

Our study highlights the significance of examining individual ensemble members rather than solely relying on the ensemble mean in order to gain a comprehensive understanding of a climate model's characteristics and forecasting abilities. Specifically, we find that the prevalent issue of a strong ENSO-ISMR relationship in many climates models may not necessarily stem from a fundamental lacuna within the model but rather arises from the methodology employed in calculating the ensemble mean.

5 Open Research

Data availability

The rainfall data utilized in the study are obtained from the IMD (`https://imdpune` `.gov.in/ndc_new/Request.html`) and GPCP (`https://psl.noaa.gov/data/gridded/data` `.gpcp.html`). The SST dataset is accessible at `https://psl.noaa.gov/data/gridded/` `data.noaa.ersst.v5.html`. The CFSv2 simulations of model M1 are based on following the experimental setup employed by Rajendran et al. (2021) and Singhai et al. (2023), while the NCEP-CFSv2 retrospective runs used for verification purposes are generated by Saha et al. (2010) and are available through NCEP at `https://www.ncdc.noaa.gov/data-access/` `model-data/model-datasets/climate-forecast-system-version2-cfsv2`.

References

Atger, F. (1999). The skill of ensemble prediction systems. *Monthly Weather Review*, *127*(9), 1941–1953.

Cash, B. A., Barimalala, R., Kinter, J. L., Altshuler, E. L., Fennessy, M. J., Manganello, J. V., . . . Vitart, F. (2017). Sampling variability and the changing enso–monsoon relationship. *Climate Dynamics*, *48*, 4071–4079.

Chakraborty, A., & Singhai, P. (2021). Asymmetric response of the Indian summer monsoon to positive and negative phases of major tropical climate patterns. *Scientific reports*, *11*(1), 1–13.

Charney, J. G., & Shukla, J. (1981). Predictability of monsoons. *Monsoon dynamics*, 99–110.

Chattopadhyay, R., Rao, S. A., Sabeerali, C., George, G., Rao, D. N., Dhakate, A., & Salunke, K. (2016). Large-scale teleconnection patterns of Indian summer monsoon as revealed by CFSv2 retrospective seasonal forecast runs. *International Journal of Climatology*, *36*(9), 3297–3313.

Das, R. S., Rao, S. A., Pillai, P. A., Srivastava, A., Pradhan, M., & Ramu, D. A. (2022). Why coupled general circulation models overestimate the ENSO and Indian summer monsoon rainfall (ismr) relationship? *Climate Dynamics*, *59*(9-10), 2995–3011.

George, G., Rao, D. N., Sabeerali, C., Srivastava, A., & Rao, S. A. (2016). Indian summer monsoon prediction and simulation in CFSv2 coupled model. *Atmospheric Science Letters*, *17*(1), 57–64.

Gershunov, A., Schneider, N., & Barnett, T. (2001, June). Low-frequency modulation of the ENSO–indian monsoon rainfall relationship: Signal or noise? *Journal of Climate*, *14*(11), 2486–2492. Retrieved from `https://doi.org/10.1175/1520-0442(2001)` `014<2486:lfmote>2.0.co;2` doi: 10.1175/1520-0442(2001)014⟨2486:lfmote⟩2.0.co;2

He, L., Zhou, T., & Chen, X. (2022). South asian summer rainfall from CMIP3 to CMIP6 models: biases and improvements. *Climate Dynamics*, 1–13.

Huang, B., Thorne, P. W., Banzon, V. F., Boyer, T., Chepurin, G., Lawrimore, J. H.,

... Zhang, H.-M. (2017). NOAA extended reconstructed sea surface temperature (ERSST), version 5. *NOAA National Centers for Environmental Information*, *30*, 8179–8205.

Huffman, G. J., Adler, R. F., Bolvin, D. T., & Gu, G. (2009). Improving the global precipitation record: GPCP version 2.1. *Geophysical Research Letters*, *36*(17).

Kim, H.-M., Webster, P. J., Curry, J. A., & Toma, V. E. (2012). Asian summer monsoon prediction in ECMWF System 4 and NCEP CFSv2 retrospective seasonal forecasts. *Climate Dynamics*, *39*, 2975–2991.

Krishnamurthy, V. (2018). Seasonal prediction of South Asian monsoon in CFSv2. *Climate Dynamics*, *51*(4), 1427–1448.

Kucharski, F., Bracco, A., Yoo, J., & Molteni, F. (2007). Low-frequency variability of the Indian monsoon–ENSO relationship and the tropical Atlantic: The "weakening" of the 1980s and 1990s. *Journal of Climate*, *20*(16), 4255–4266.

Kucharski, F., Bracco, A., Yoo, J., & Molteni, F. (2008). Atlantic forced component of the Indian monsoon interannual variability. *Geophysical Research Letters*, *35*(4).

Leutbecher, M., & Palmer, T. N. (2008). Ensemble forecasting. *Journal of computational physics*, *227*(7), 3515–3539.

Molteni, F., Buizza, R., Palmer, T. N., & Petroliagis, T. (1996). The ECMWF ensemble prediction system: Methodology and validation. *Quarterly journal of the royal meteorological society*, *122*(529), 73–119.

Palmer, T. N. (2000). Predicting uncertainty in forecasts of weather and climate. *Reports on progress in Physics*, *63*(2), 71.

Parthasarathy, B., Munot, A., & Kothawale, D. (1994). All-India monthly and seasonal rainfall series: 1871–1993. *Theoretical and Applied Climatology*, *49*(4), 217–224.

Pillai, P. A., Rao, S. A., Srivastava, A., Ramu, D., Pradhan, M., & Das, R. S. (2021). Impact of the tropical Pacific SST biases on the simulation and prediction of indian summer monsoon rainfall in CFSv2, ECMWF-System4, and NMME models. *Climate Dynamics*, *56*, 1699–1715.

Rajeevan, M., Bhate, J., Kale, J., & Lal, B. (2006). High resolution daily gridded rainfall data for the Indian region: Analysis of break and active monsoon spells. *Current Science*, 296–306.

Rajendran, K., Surendran, S., Varghese, S. J., & Chakraborty, A. (2021). Do seasonal forecasts of indian summer monsoon rainfall show better skill with February initial conditions? *Current Science (00113891)*, *120*(12).

Rajendran, K., Surendran, S., Varghese, S. J., & Sathyanath, A. (2022). Simulation of indian summer monsoon rainfall, interannual variability and teleconnections: evaluation of CMIP6 models. *Climate Dynamics*, *58*(9-10), 2693–2723.

Ramu, D. A., Chowdary, J. S., Ramakrishna, S., & Kumar, O. (2018). Diversity in the representation of large-scale circulation associated with enso-indian summer monsoon teleconnections in CMIP5 models. *Theoretical and applied climatology*, *132*, 465–478.

Rasmusson, E. M., & Carpenter, T. H. (1983). The relationship between eastern equatorial Pacific sea surface temperatures and rainfall over India and Sri Lanka. *Monthly Weather Review*, *111*(3), 517–528.

Sabeerali, C., Ajayamohan, R., Bangalath, H. K., & Chen, N. (2019). Atlantic Zonal Mode: An emerging source of Indian summer monsoon variability in a warming world. *Geophysical Research Letters*, *46*(8), 4460–4467.

Saha, S., Moorthi, S., Pan, H.-L., Wu, X., Wang, J., Nadiga, S., . . . others (2010). The ncep climate forecast system reanalysis. *Bulletin of the American Meteorological Society*, *91*(8), 1015–1058.

Saha, S., Moorthi, S., Wu, X., Wang, J., Nadiga, S., Tripp, P., . . . others (2014). The NCEP climate forecast system version 2. *Journal of climate*, *27*(6), 2185–2208.

Shukla, J., & Wallace, J. (1983). Numerical simulation of the atmospheric response to equatorial Pacific sea surface temperature anomalies. *Journal of the Atmospheric Sciences*, *40*(7), 1613–1630.

Shukla, R. P., & Huang, B. (2016). Mean state and interannual variability of the indian summer monsoon simulation by NCEP CFSv2. *Climate Dynamics*, *46*, 3845–3864.

Singh, B., Cash, B., & Kinter III, J. L. (2019). Indian summer monsoon variability forecasts in the North American multimodel ensemble. *Climate dynamics*, *53*(12), 7321–7334.

Singhai, P., Chakraborty, A., Rajendran, K., & Surendran, S. (2023). Why is the indian summer monsoon in CFSv2 hypersensitive to moisture exchange with the Pacific Ocean? *Climate Dynamics*, 1–17.

Tippett, M. K., Trenary, L., DelSole, T., Pegion, K., & L'Heureux, M. L. (2018). Sources of bias in the monthly cfsv2 forecast climatology. *Journal of Applied Meteorology and Climatology*, *57*(5), 1111–1122.

Weisheimer, A., Palmer, T., & Doblas-Reyes, F. (2011). Assessment of representations of model uncertainty in monthly and seasonal forecast ensembles. *Geophysical Research Letters*, *38*(16).